Desalination 308 (2013) 63–72

Contents lists available at SciVerse ScienceDirect

Desalination

journal homepage: www.elsevier.com/locate/desal

Self-adaptive feed flow reversal operation of reverse osmosis desalination

Han Gu, Alex R. Bartman, Michal Uchymiak, Panagiotis D. Christofides, Yoram Cohen *

Department of Chemical and Biomolecular Engineering and Water Technology Research Center, University of California, Los Angeles, 420 Westwood Plaza, Chemical Engineering Offices, Boelter Hall 5531, Los Angeles, CA 90095, USA

HIGHLIGHTS

► Self-adaptive mode of feed-flow reversal (FFR) was developed for RO desalting.
► FFR was triggered via mineral scale detection using an external membrane monitor.
► Membrane permeability was recovered after each FFR cycle.
► Scale-free cyclic FFR RO operation was achieved without use of anticalants.
► Continuous permeate production was attained under gypsum supersaturation conditions.

GRAPHICAL ABSTRACT

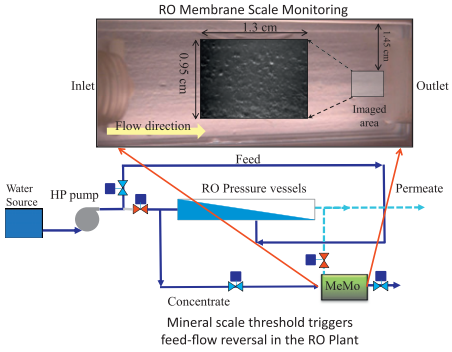

ARTICLE INFO

Article history:
Received 23 June 2012
Received in revised form 26 July 2012
Accepted 28 July 2012
Available online 5 September 2012

Keywords:
Feed flow reversal
Mineral scale detection
Reverse osmosis
Brackish water desalination
Membrane monitor

ABSTRACT

The technical feasibility of operating a spiral-wound RO plant in a cyclic mode of feed-flow reversal (FFR) was evaluated for brackish water desalting under conditions of high mineral scaling propensity. Scale-free and continuous permeate productivity was demonstrated, with calcium sulfate as the model scalant, in an automated spiral-wound RO pilot system in which FFR was triggered by scale detection in an external membrane monitor (MeMo). Real-time detection of mineral scaling in an external RO MeMo cell, receiving its feed from the concentrate of the RO plant tail element, enabled cyclic FFR operation in a self-adaptive mode accomplished by feed-back RO plant control in which permeate productivity was maintained. Membrane permeability was restored after each FFR cycle even with the initiation of membrane cleaning (i.e., via FFR) after a measurable level of scale formation in the MeMo and spiral-wound RO pilot. FFR cycle periods varied in length given the stochastic nature of crystal nucleation on the membranes in both the RO plant and in the MeMo RO cell. Scale-free FFR operation was demonstrated, without anticalant addition, with the RO plant operating (up to 81% recovery) such that the gypsum saturation index was up to 3.45 at the membrane surface of the tail element.

1. Introduction

Reverse osmosis (RO) membrane desalination technology has advanced considerably since its early development to become a viable approach for the generation of new water supplies from seawater and inland brackish water [1–6], as well as for water reuse [7]. Although RO is a relatively mature technology, brackish water desalination remains a challenge due to the need for high recovery operation which is desirable in inland locations in order to minimize concentrate management costs; however, the recovery levels achievable by RO desalination are typically limited by membrane mineral scaling due to precipitation of sparingly water soluble salts. As product water recovery increases along the RO modules, the concentration of mineral salts on the feed-side and near the RO membrane surface

* Corresponding author. Tel.: +1 310 825 8766.
E-mail address: yoram@ucla.edu (Y. Cohen).

0011-9164/$ – see front matter © 2012 Elsevier B.V. All rights reserved.
http://dx.doi.org/10.1016/j.desal.2012.07.041

can increase to levels exceeding their solubility limits. As a consequence mineral scale forms due to surface crystallization of these mineral salts and/or the deposition of their bulk-formed crystals onto the membrane surface. The resulting mineral surface scale leads to water permeate flux decline and potential membrane damage [8], thereby limiting recovery and increasing water production cost.

Sparingly soluble mineral salts such as calcium sulfate dihydrate (also known as gypsum), calcium carbonate (or calcite) and barium sulfate (or barite) are three of the common problematic mineral scalants encountered in inland brackish water desalination [8,9]. In general, the supersaturation level of the mineral scalant of concern can be expressed in terms of the saturation indices (SI) defined as $SI_y = IAP_y/K_{sp,y}$, where IAP_y and $KP_{sp,y}$ are the ion activity and solubility products of mineral scalant y, respectively. Calcite solubility is pH dependent and thus lowering of its saturation index (i.e., increasing solubility to suppress calcite scaling) can be achieved via pH adjustment of the RO feed [8], while in contrast gypsum and barite solubilities are pH insensitive [10]. Antiscalants can be effectively utilized to suppress mineral scaling for $CaCO_3$, $SrSO_4$, $CaSO_4$, and SiO_2 provided that the mineral salt saturation levels (at the membrane surface) do not exceed the recommended levels (e.g., $SI_{CaCO3} \leq 60$, $SI_{SrSO4} \leq 8$, $SI_{CaSO4} \leq 2.3$, $SI_{SiO2} \leq 1$, [10]. Therefore, even with the use of antiscalants product water recovery is limited [10]. Moreover, antiscalant use increases the cost of RO desalination [2,11,12] and its applied dose may be limited in certain conditions due to the potential for increased biofouling propensity at elevated antiscalant dosage [11].

An alternative approach that has been proposed for averting membrane mineral scaling, while eliminating or reducing antiscalant use, is that of operating (cross flow) RO desalination elements in "Feed Flow Reversal" (FFR) [13,14]. In the FFR approach (Fig. 1), as feed flows in the normal forward flow (NFF) mode, feed water enters the spiral-wound membrane module from its "normal" feed side. Salt concentrations then increase axially along the feed channel (with increased recovery) and to a larger degree at the membrane surface as a consequence of concentration polarization (CP) [15]. When the mineral salt scalant concentration exceeds saturation ($SI > 1$), scaling is expected to occur first in the downstream area of the feed-channel (i.e., toward the "brine" exit zone). Once the scaling level reaches a specific threshold feed flow reversal (FFR) is initiated, whereby the raw feed is redirected to enter through the previously designated outflow end, while the previous "entrance" end becomes the "exit" end of the module. As the entrance "end" (scaled in the previous NFF period) is exposed to the undersaturated raw feed, mineral salts on

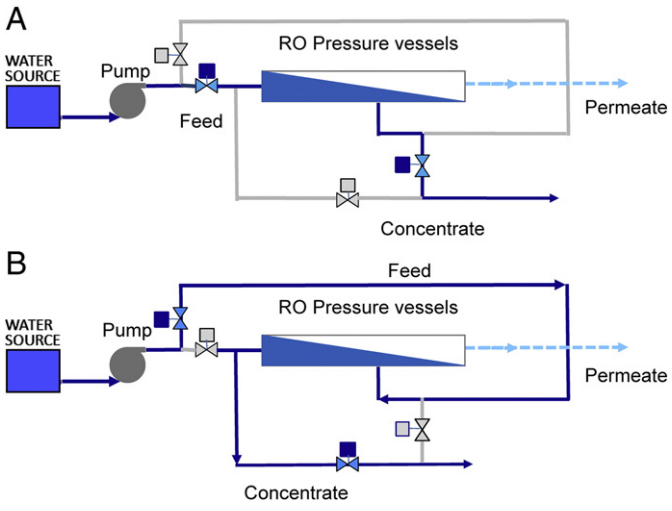

Fig. 1. Schematic of RO operation in (A) normal feed flow mode (NFF), and (B) feed flow reversal (FFR).

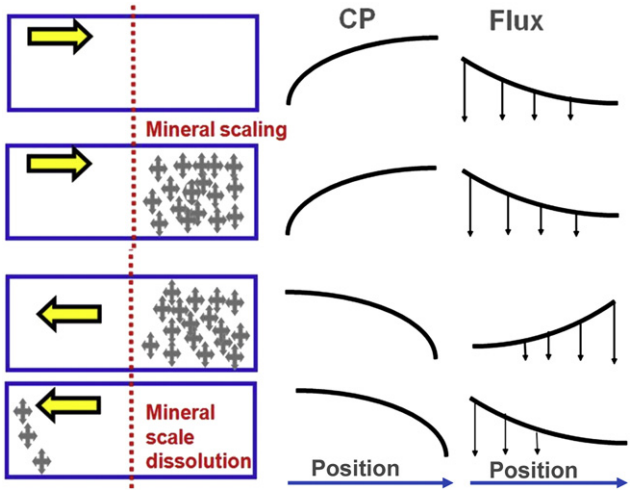

Fig. 2. Illustrations of the basic concept of feed flow reversal operation. Periodic reversal of the flow direction reverses the CP profile in the RO elements exposing scaled areas to undersaturated solution thereby resulting in dissolution of mineral crystals.

the membrane surface are dissolved (given that the driving force for precipitation has been reversed; [16]). The above mode of periodic switching of the flow direction (in the membrane module) disrupts and reverses the CP profile (Fig. 2) in the RO feed channel and results in cycling scale dissolution/formation. The above operational model can be envisioned as one of resetting the apparent crystallization "induction time" defined as the time between the start of system operation and the time the first crystal begins to form on the membrane surface [8,13]. It is noted that, unlike cleaning methods such as osmotic backwash [17] and high-salinity solution direct osmosis (DO) backwash [18], FFR operation does not interrupt permeate production. It should be recognized that the onset of mineral scaling may vary over FFR cycles since nucleation of mineral crystallization is a stochastic process and also because water feed quality can vary temporally with respect to its mineral scaling propensity. Given the above, a robust implementation of FFR requires real-time mineral scale monitoring to enable automated and self-adaptive FFR triggering that can be effectively integrated with process control to establish the frequency and duration of FFR cycles.

Triggering of FFR using an ex-situ scale observation detector (EXSOD) was previously demonstrated [8,16] for mitigating gypsum scaling in a small brackish water RO pilot plant (up to 3 m^3/day capacity). In this approach, a flat sheet RO membrane coupon is placed in a transparent plate-and-frame RO (PFRO) cell for direct real-time membrane surface imaging [8,19] for monitoring scale formation. It was shown that FFR triggering can be achieved sufficiently early by adjusting the flow through the PFRO cell to achieve the desired level of solution supersaturation at the membrane surface. Improved mineral scale detection and evaluation of the evolution of crystal nucleation, via automated image analysis, was subsequently developed [20] for application of the EXSOD type scale detection system. Also, the use of model-predictive control of FFR operation for RO desalting was later proposed [21] in order to avoid pressure fluctuation and water hammer when reversing the feed flow. It is noted that earlier studies on RO operation in FFR mode [8,14,16] have not demonstrated self-adaptive control (i.e., in terms of FFR cycle frequency and duration) over multiple operational cycles. Also, FFR operation was not demonstrated at significant scaling level of the RO membranes to unambiguously establish the reversal of mineral scaling (i.e., effective cleaning and restoration of membrane permeability).

In the preset study, the technical feasibility of RO FFR operation was evaluated experimentally in a multi-cycle FFR operation of a

Table 1
Composition and properties of the RO feed.

Analytes	Concentration	
Ca^{2+}	10	mM
Na^{+}	20	mM
SO_4^{2-}	10	mM
Cl^{-}	20	mM
TDS (mg/L)	1779	mg/L
SI_{gypsum} (at 25 °C)	0.454	
pH	7.6	

spiral-wound RO desalination pilot system [16]. Mineral scale monitoring and FFR triggering were achieved via an improved surface scale monitor (MeMo) and real time image analysis capability [20]. Mineral salt crystallization is a stochastic process and thus the present work demonstrates self-adaptive FFR operation of a fully automated RO plant in which FFR was triggered by the MeMo plant, without antiscalant dosing and effective permeability recovery post scaling.

2. Experimental

2.1. Materials and model solutions

Model feed solutions (Table 1) were prepared using analytical grade calcium chloride dihydrate and anhydrous sodium sulfate (Fisher Scientific, ACS grade, Pittsburgh, PA) in deionized (DI) water, with the solution pH maintained at 7.4. The feed solution had a salinity of 1779 mg/L total dissolved solids (TDS) and a gypsum ($CaSO_4 \cdot 2H_2O$) saturation index (SI_g) of 0.454. The solution was undersaturated with respect to gypsum to avoid bulk crystallization (Table 1) in the feed reservoir and in the piping network feeding the RO plant.

The membrane coupons had an active surface area of 26.9 cm^2, average water permeability of 1.56 L/(m^2-h-bar) and an observed salt rejection of 92.5% (at 25.8 bar). The spiral-wound membranes utilized in the RO system (Dow Filmtec XLE-2540, The Dow Chemical Company, Midland, MI) were 2.5 inch (outer diameter) elements and 40 inch long with an average surface area of 2.601 m^2. These membranes had water permeability of 4.57 ± 0.11 L/(m^2-h-bar) and an average observed rejection of 97.7% determined at 18.7 bar and 63% recovery for an 11,380 mg/L NaCl solution. Each membrane was loaded into a separate pressure vessel with six membranes connected in series. It is noted that for each set of experiments, newly conditioned flat sheet membrane coupons were used in the membrane mineral scale monitor.

2.2. RO pilot system (M3) and mineral scale monitor

RO operation in FFR mode was investigated using the UCLA spiral-wound mini-mobile-modular (M3) RO system [2,4,6] having permeate production capacity of up to 1.2 m^3/h (7560 gallons/day) for brackish water (5000 mg/L TDS) operating at 75% recovery and up to 0.64 m^3/h (4058 gallons/day) for seawater desalination (at recovery of 40%). However, in the M3 configuration used in the present study only six spiral-wound elements (instead of the full capacity of 18 elements) were installed in series, (each housed in a separate pressure vessel); PV1–PV6 rated up to 68.9 bar (1000 psi). The system was operated in a total recycle mode with the permeate and concentrate streams returned to the feed tank. A refrigerated recirculator (Model CFT-75 Neslab Instruments Inc. Newington, NH) was used (along with a 1.27 cm outer diameter cooling coil of 1.7 m linear length) to control the feed temperature to 25 °C ± 1 °C. Feed water to the RO unit from a 450 L tank is first directed using low pressure intake pumps (Model JM3460-SRM, Sea Recovery, Carson, CA) through a sequence of cartridge microfilters (5 μm, 0.45 μm and 0.2 μm; 08P GIANT, pleated 177 polypropylene filter cartridges,

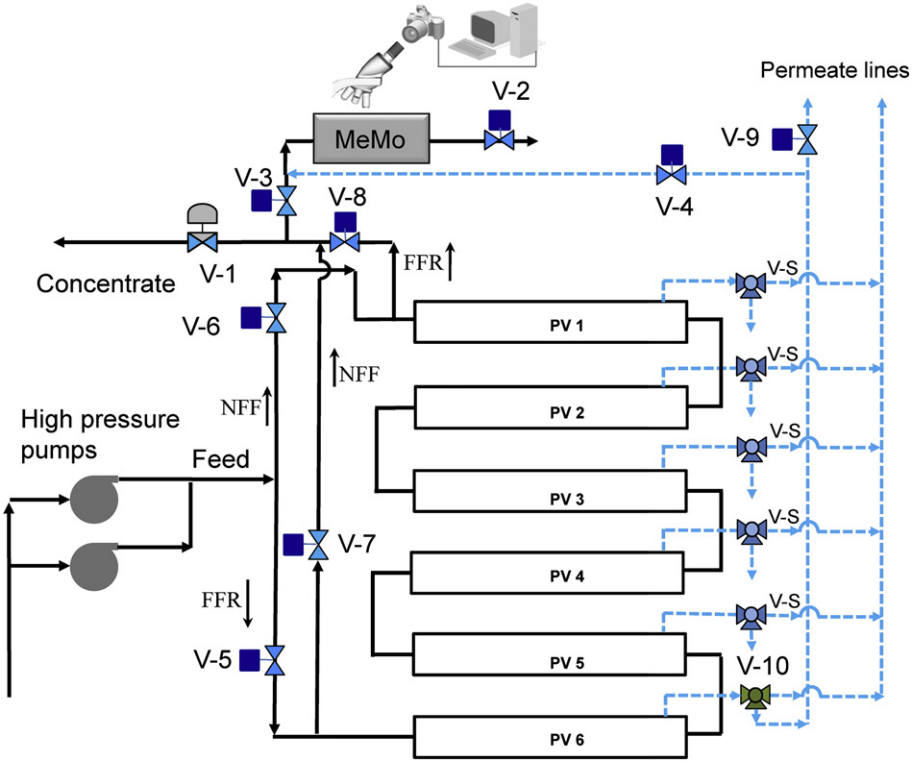

Fig. 3. Schematic diagram of the M3–MeMo flow reversal system showing the location and arrangement of actuated valves, pressure vessels and permeate collection network (dashed lines). NFF and FFR represent normal feed flow and feed flow reversal direction, respectively, with the arrows indicating the corresponding flow directions. (Note: permeate sampling valves are labeled as V-S).

Table 2
Valve configuration during RO system operation in normal feed flow and feed flow reversal[a].

	V-1	V-2	V-3	V-4	V-5	V-6	V-7	V-8	V-9
Normal feed flow	Unchanged	MeMo NFF setting	MeMo NFF setting	Closed	Open	Closed	Closed	Open	Open
Feed flow reversal	Unchanged	MeMo cleaning setting	MeMo cleaning setting	Open	Closed	Open	Open	Closed	Closed

Note: valves V-4 and V-10 are open when the MeMo undergoes cleaning with permeate water (Fig. 3).
[a] Valves V-1, V-2, and V-3 are actuated control valves and are not adjusted during transition between NFF and FFR modes.

Keystone Filter, Hatfield, PA). An inline turbidity meter (Micro TOL 20055, HF Scientific, Fort Myers, FL) was used to monitor the stream exiting the feed pre-filtration system. The feed to the RO was provided with two positive-displacement high pressure pumps (Danfoss Model CM 3559, 3HP, 3450RPM, Baldor Reliance Motor, Sea Recovery Corp. Carson, CA) controlled by variable frequency drives (VFDs) (Model FM50, TECO Fluxmaster, Round Rock, TX). The feed and retentate pressures are monitored using two pressure transducers (0–1000 psig, Model PX409-1.0KG10V Omega, Stamford, CT). An electrically actuated needle valve (valve V-1) (model VA8V-7-0-10, ETI Systems, Carlsbad, CA) on the retentate stream of the M3 RO system, along with the pump VFD, enabled the control of the retentate flow rate and pressure in the RO unit using a model-based controller [21].

Permeate and retentate streams of the M3 were also monitored with in-line via conductivity sensors, and conductivity/resistivity sensor electronics (Signet 2839 to 2842 and Signet 2850, George Fischer Signet, Inc. El Monte, CA) and pH sensor (DryLoc pH electrodes 2775, George Fischer Signet, Inc. El Monte, CA). Real-time calcium ion concentration in the concentrate stream, for the present feed solution, was determined by correlating calcium ion concentration with the measured conductivity of the RO concentrate, based on simulation results from a multi-electrolyte thermodynamic simulator [22]:

$$\left[Ca^{2+}\right] = \left(\frac{EC}{150.7}\right)^{1.265} \quad (1)$$

$$SI_g = 59.77\left[Ca^{2+}\right] - 0.1289 \quad (2)$$

in which EC is the solution conductivity (mS), $[Ca^{2+}]$ is the calcium ion concentration (M), and SI_g is the gypsum saturation index. The above correlations is applicable to the SI range of 0.48–5.12 for a calcium ion concentration range of 15–80 mM, which covers the range relevant in the present study.

Feed flow reversal through the feed/retentate channel of the RO membranes was facilitated via a series of direct acting two-way solenoid valves (GC valves model HS4GF15A24GC, Simi Valley, CA) (Fig. 3). The solenoid valve network (valves V-5, V-6, V-7, and V-8) controlled the direction of the feed water flow to allow for feed channel flow reversal. The valve configurations for the normal feed flow (NFF) and FFR modes are provided in Table 2 and details of the operation are provided in Section 2.3. FFR was triggered by a preset scaling threshold in the MeMo scale monitoring system (Fig. 4). The MeMo PFRO cell received as its feed the RO retentate (i.e., concentrate) from the high pressure side stream (upstream from the retentate valve) of the RO M3 system (Fig. 3), on the exit side of its last (sixth) pressure vessel (PV6 during NFF and PV6 during FFR).

The MeMo system was equipped with a semi-transparent plate-and-frame RO (PFRO) flow cell with an optical window and a microscope interfaced with a high resolution digital camera. The active membrane area was 8.1 cm × 3.16 cm with a 0.254 cm feed channel height. Selected areas of the membrane or the entire membrane coupon can be imaged aided with near dark-field illumination to provide high contrast imaging of surface crystals. For

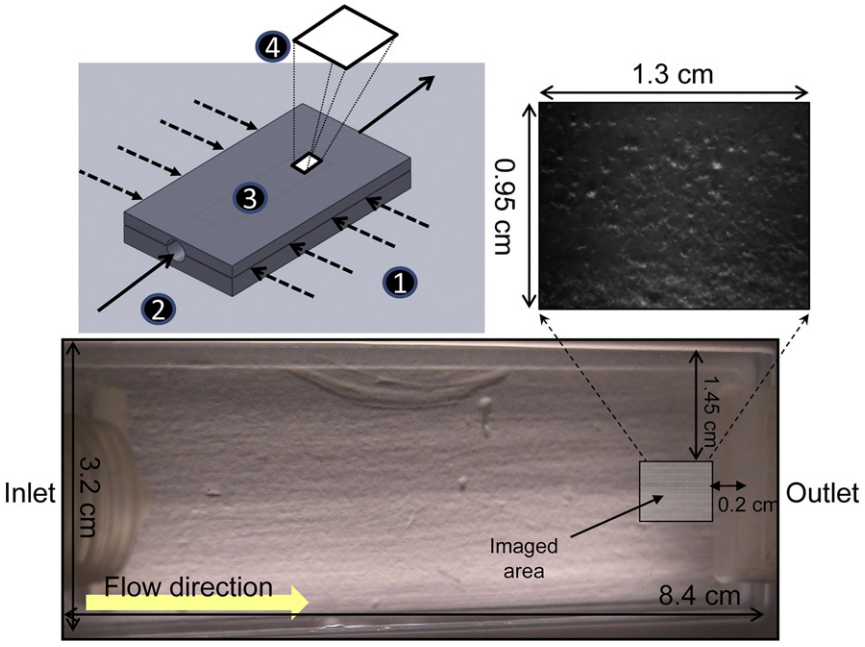

Fig. 4. Membrane monitor (MeMo) cell: 1) incident light, 2) feed water stream inlet, 3) membrane coupon. An example of a scaled image of a small portion of a monitored location near the exit region of the RO cell is shown above the expanded image of the membrane coupon in the MeMo cell (adapted from [20]).

the purpose of FFR triggering the imaged area of the MeMo flow cell (1.3 cm × 0.95 cm) was set 0.32 cm away from the center line of the viewing window and 6.5 cm downstream from the feed inlet to avoid areas of diminished mass transfer and recirculation eddies [12,15]. The inlet pressure to the MeMo flow cell was monitored by a pressure transducer (PX 303-500G5V Omega, Stamford, CT) and permeate flow rate was measured using a digital flow meter (Model 1000, Fisher Scientific, Pittsburgh, PA). Feed and permeate conductivities were monitored with an online conductivity meter (Model WD-35607-30, Oakton Research, Vernon Hills, IL). Additional details of the MeMo system are provided elsewhere [20,23].

The MeMo membrane surface was continuously monitored with images recorded at regular time intervals (typically 5 min) and subsequently analyzed (online) using specially developed automated image analysis software [16,20]. Images were analyzed for the fractional mineral scale surface coverage and the crystals count in the observation area [20]. Once the surface scale coverage (or number of crystals) reached the specified threshold value (Fig. 5), a signal (analog or digital) was transmitted to the RO control system to initiate the FFR mode of operation and MeMo cleaning in preparation for scale monitoring in the subsequent NFF cycle. After a specified period of operation in the FFR mode (Fig. 5, typically 5 min less than the NFF period; [20], the flow was again reversed to the NFF mode.

Gypsum saturation level at the MeMo membrane surface, SI_{gm}, was calculated for the given flow conditions (pressure, inlet velocity, and salinity) from the CP modulus (i.e., $CP = C_m/C_b$, where C_m and C_b are the concentrations at the membrane surface and in the bulk of the flow channel, respectively) for the cell geometry. The CP profile was determined using a previously developed numerical 3-D CFD model for the MeMo cell geometry [15]. Feed flow rate and transmembrane pressure in the MeMo cell were adjusted so as to set the desired SI_{gm} level at the membrane surface relative to the SI_{gm} in the tail spiral wound element (membrane surface at the exit region) in the M3 system. Concentrations of the scaling species at the membrane surface in the M3 RO tail element were estimated based on the ROSA software [24] approach, where the CP modulus was determined from $CP = C_m/C_b = e^{[k \cdot 2Y/(2-Y)]}$, where Y is the recovery for the spiral wound RO element, k is a proportionality constant that depends primarily on membrane element length (taken to be 0.7 for the 40 inch spiral wound elements used in this study), and C_m and C_b are the concentrations at membrane surface and in the bulk of the feed channel, respectively [25].

2.3. Self-adaptive feed flow reversal operation of RO system

In a normal feed flow (NFF) (i.e., flow from PV1 to PV6), valves V-5 and V-8 are open, while valves V-4, V-6, and V-7 are closed (Table 2 and Fig. 3). During this period, the MeMo system is at a scale-detection mode and where it is fed with a side stream of RO concentrate from the tail element. It is noted that the pressure and flow rate for the MeMo cell feed are adjusted with the aids of valves V-2 and V-3. During the subsequent FFR operation (i.e., feed flow from PV6 to PV1), valves V-4, V-6 and V-7 are open while valves V-5 and V-8 are closed. In this mode, the MeMo system is cleaned (i.e., mineral crystals are dissolved) by low pressure permeate water produced by the lead element of the M3 system (typically at permeate cross flow rate of ~10 cm/s and pressure of ~0.345 bar). The process of switching from NFF to FFR mode is completed within ~2 s after the control system receives the triggering signal. A proportional integral (PI) controller is utilized in the M3 system to adjust the retentate valve position (V-1) in order to maintain the feed pressure after the switching of the solenoid valves (Table 2) to the FFR configuration (and also when switching from FFR back to NFF mode).

Automated RO desalting operation in FFR mode was demonstrated via three distinct operational scenarios (Table 3) using the spiral-wound M3 RO pilot plant [20]. In all cases the feed solution was undersaturated with respect to gypsum while being oversaturated ($SI_{gm} = 2.74–3.65$) at the membrane surface for both the M3 tail element and at the MeMo RO cell. In the first test, the M3 was operated in normal feed flow at an initial water recovery level of 69% ($SI_{gm,\,M3} = 2.74$). Mineral scaling was monitored with the MeMo with the initial conditions set such that $SI_{gm,MeMo} = 2.87$. In this operational

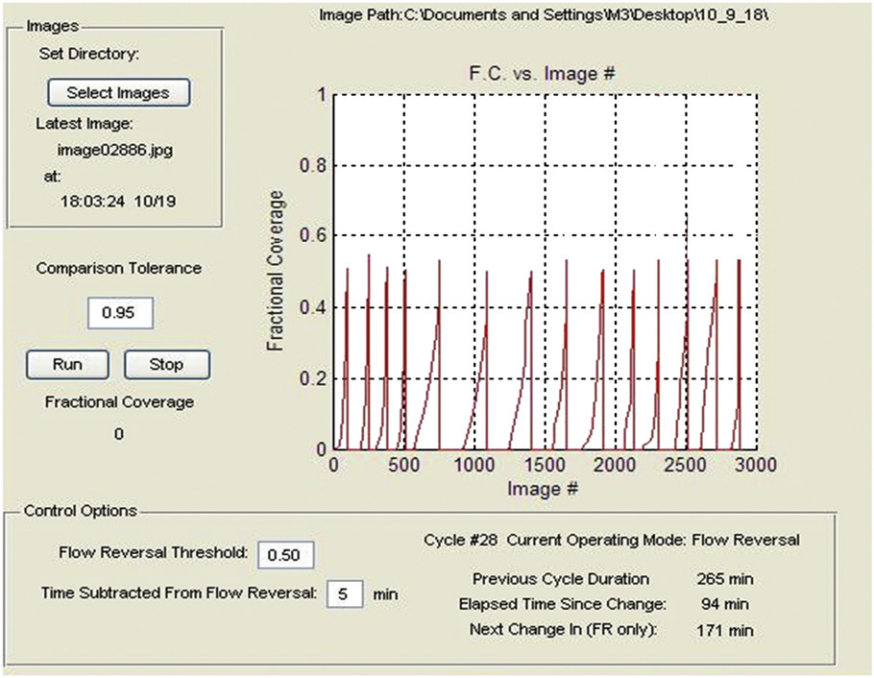

Fig. 5. Screenshot of the user interface of the online image tracking software during the multi-cycle FFR operation (Test #2) showing the calculated fractional surface scale coverage. The Run and Stop buttons initiate and stop, respectively, the online image analysis program. Control Options include: Flow Reversal Threshold indicates (pre-set fractional coverage for triggering flow reversal), time for NFF (i.e., FFR time reduced by "time subtracted from flow reversal").

Table 3
Experimental conditions for gypsum RO membrane scaling experiments.

Test	M3 RO system transmembrane pressure in bar (psi)	M3 RO system recovery (%)	Gypsum saturation index			FFR triggering threshold (% surface coverage)	Duration (h)
			Feed (bulk)	M3[(b)]	MeMo[(b)]		
#1[(a)]	11.6 (168)	69.1	0.44	2.74	2.87	None	4
#2	11.6 (168)	69.1	0.44	2.76	2.87	50	88
#3	13.6 (197)	81.1	0.37	3.45	3.65	65	80

[(a)] Operation without feed flow reversal.
[(b)] Initial gypsum saturation indices at the membrane surfaces for the M3 tail element and for the MeMo RO cell.

scenario the MeMo was operated at just slightly above the saturation level encountered in the M3 tail element (Table 3); this enabled evaluation of early scale detection relative to the monitored overall and tail element flux decline in the M3 plant. This test also served to establish a reasonable mineral scaling threshold (in the MeMo cell) for triggering the RO plant switch from NFF to FFR mode of operation. At the termination of the above test, the M3 system was cleaned by pumping DI water in both the forward and reverse directions. Complete scale removal (i.e., permeate flow rate recovered to its original level, and no scale observed within viewable area in the MeMo cell) was achieved after 1.5 h.

FFR evaluation in the second test was carried out over a period of 88 h with the M3 plant product water recovery set at 69%. The level of gypsum supersaturation at the membrane surface was set as in the first test (Table 3) with the scaling threshold in the MeMo (for triggering FFR) set to surface scale coverage of about 50%; this scaling threshold was equivalent to about 5% flux decline in the M3 tail element as evaluated from the test without FFR (i.e., Test #1, Table 3). Membrane cleaning efficiency (i.e., removal of surface scale) via the cyclic FFR process was determined based on the percent flux recovery for the tail element (F_R), at the same initial transmembrane pressure, calculated as $F_R = F_i/F_o$, where F_i and F_o are the normalized permeate flux values at the end of the previous NFF period and at the beginning of the cycle (or 1st cycle) for each FFR cycle.

In the subsequent FFR evaluation (Test #3, Table 3), the M3 pilot system was operated for a period of 80 h at a higher water recovery of 81% and thus a higher gypsum saturation index ($SI_{gm,M3} = 3.45$) at the membrane surface of the tail element. For this test, the MeMo cell was operated such that $SI_{gm,MeMo} = 3.65$ and the scaling threshold for FFR triggering was increased to 65% surface area scale coverage. The purpose of above scenario was to evaluate the impact of a less stringent FFR triggering threshold on the FFR cycle time and permeate flux recovery.

3. Results and discussion

3.1. Evaluation of early scale detection in the M3 plant

Adequacy of the MeMo scale monitoring for early detection of the onset of mineral scaling in the RO pilot plant was first assessed in Test #1 (Table 3). The M3 operated at 69% recovery such that the level of gypsum saturation at the membrane surface of the M3 tail element was above the saturation ($SI_{gm} = 2.74$). Surface scaling was observed in the MeMo cell with rapid buildup of mineral scale in the monitored

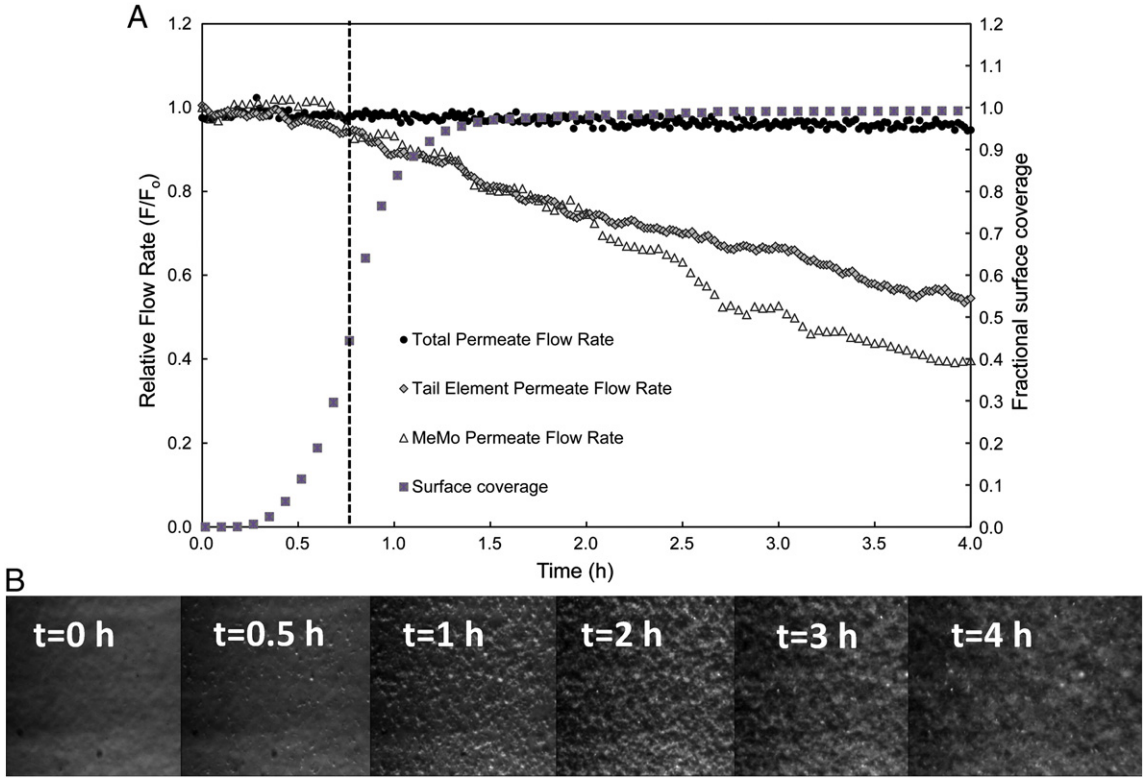

Fig. 6. (A) M3 operation at 69% recovery, with MeMo scale monitoring, in normal feed flow (Test 1; Table 3) under mineral scaling conditions, showing the relative permeate flow rates (total and PV6 tail element for the M3 system and for the MeMo cell) along with crystal surface coverage in the MeMo cell. ($F_o = 6.59$, 0.477 and 0.27×10^{-3} L/min for the total M3, PV6 and MeMo, respectively). The vertical dashed line indicates the time at which the surface coverage in the MeMo cell reached 50%. (B) Selected membrane surface images in the monitored area of the MeMo cell.

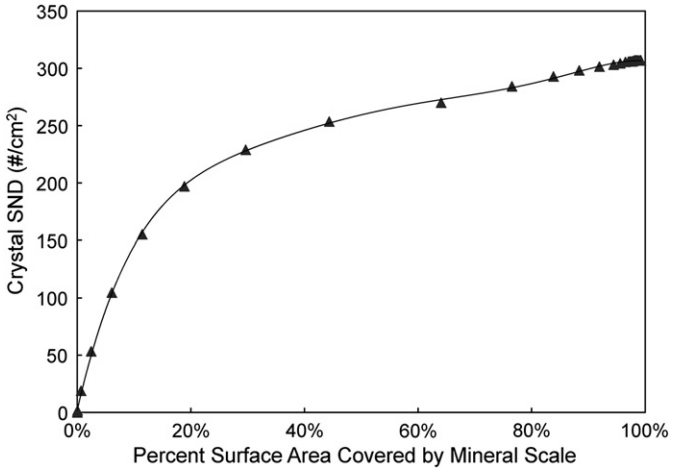

Fig. 7. Correlation of crystal site number density (SND) with the percent mineral scale coverage in the MeMo viewing area for Test #1 (M3 operation at 69% recovery, $SI_{gm} = 2.74$, Table 3).

area (Fig. 6A and B) reaching about 100% in 1.5 h. During the same period the total M3 permeate flow did not reveal significant flux decline with only up to ~4% flux decline over the 4 h period of Test #1, while significant flux decline was observed for both the M3 tail element (PV6) and for the MeMo cell. Flux decline for the MeMo and for the M3 tail element paralleled each other (Fig. 6A) until a period of 2 h. At $t > 2$ h, flux decline for the MeMo was greater relative to the M3 RO tail element; this was expected since $SI_{g,m}$ at the MeMo was greater than for the M3 tail element (Table 3). With the $SI_{g,m}$ at the MeMo being only ~5% above that in the M3 system ($SI_{g,m} = 2.74$), a surface scale coverage of 50% was detected (in the MeMo monitored zone) when the M3 tail element flux declined by only 5%, with essentially no detectable overall flux decline for the RO M3 pilot. The percent of surface scale coverage in the MeMo observation region (Fig. 6A and B) increased to 100% once about 47% flux decline was reached for the M3 tail element. It is noted that only a small portion of the MeMo membrane surface (Section 2.2) was monitored near the membrane exit region; thus, the percent scaled area is significantly higher in this region of higher CP [15] relative to upstream regions of the membrane coupon. Therefore, setting the MeMo operation to a level of supersaturation just slightly above that of the tail element was adequate for mimicking the scaling trend in the M3 tail element, thereby enabling early scale detection.

In principle, one could utilize a MeMo flux decline threshold for triggering FFR. However, setting of FFR initiation based on direct observation of scaling on the membrane surface would be attained at a higher level of sensitivity, in addition to verifying that FFR triggering is indeed due to membrane scaling. It is also possible to utilize a crystal count density to establish a trigger for FFR since the surface area and crystal count density are correlated as shown in Fig. 7. Temperature and feed water composition, however, may affect the rate of crystal nucleation as well as crystal growth. Therefore, different levels of surface scale coverage can result for the same crystal number density on the membrane surface. Surface scale coverage is known to closely correlate with flux decline [19] and thus it is more reliable to set a threshold for FFR triggering based on scaled area.

3.2. Self-adaptive multi-cycle FFR operation

The reliability of the MeMo system for mineral scale detection and triggering of FFR was evaluated in Test #2 (Table 3) with the M3 system also operating at 69% recovery (overall permeate productivity of 353 L/h). The MeMo scaling threshold for FFR triggering was set to 50% surface scale coverage, which resulted in 15 FFR cycles over the 88 h test period (Fig. 8). The repeated FFR cycles show that permeate flux for PV6 was higher when it was the lead element (i.e., FFR operation) and lower when it was the tail element (NFF operation). Since the osmotic pressure of the feed water is below that of the RO concentrate, the lower osmotic pressure of the feed to PV6, during each period of FFR, resulted in a sharp permeate flux increase to

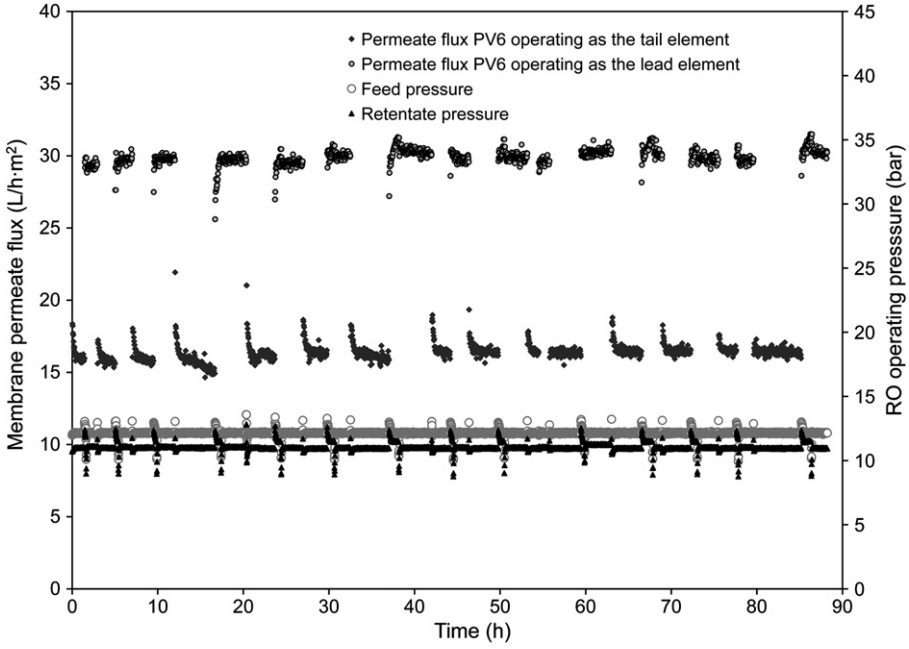

Fig. 8. Tail membrane element permeate flux (normalized w.r.t pressure) during feed flow reversal cycles and system feed pressure over the course of a multi-cycle FFR test (Test #2, M3 operation at 69% recovery, $SI_{gm} = 2.76$; Table 3). The lower permeate flux time profiles are for PV6 operating as the lead element in normal feed flow (NFF), while the lower permeate flux profiles are for PV6 as the tail element in FFR operation.

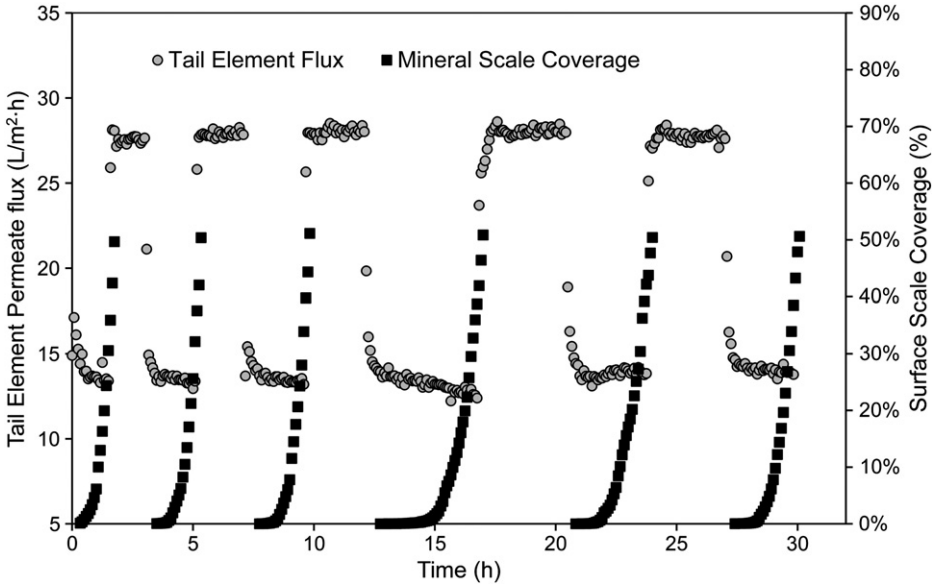

Fig. 9. Tail element (PV6) permeate flux (normalized w.r.t pressure) and percent mineral surface scale coverage (in the monitored area of the MeMo cell) for Test #2 (M3 operating at 69% recovery, $SI_{gm} = 2.76$; Table 3). The lower permeate curves designate the forward flow operation (i.e. flux of membrane element in PV6) while the top permeate flux curves denote the flow reversal operation (i.e. flux of membrane element in PV1).

~28.0–28.4 L/h·m^2 (Fig. 9 - top permeate flux curves). Since PV6 alternated between being the lead (in FFR mode) and tail (in NFF mode) element, permeate quality from this element correspondingly varied from 330 to 590 mg/L TDS to 50–230 mg/L TDS in the NFF and FFR modes, respectively. Overall, however, permeate produced by the M3 system was in the range of 210–310 mg/L TDS for both the NFF and FFR modes.

A cyclic pattern of mineral scaling was suggested by flux decline and recovery indicated by the initial flux post FFR for each new NFF cycle (Fig. 8). A more detailed view is provided in Fig. 9 which also shows the progression of scale coverage in the MeMo RO cell, along with the FFR cycle duration tracked by the M3 control system (Fig. 5). During periods of NFF operation, the normalized permeate flux from the tail element ranged from 18.2 to 17.9 L/h·m^2 at the beginning of the cycles and decreased to values ranging from 16.2 to 14.7 L/h·m^2 (depending on the cycle length). The relatively low level of permeate flux decline (about 6–13%), during each operational period in the forward flow direction, indicated that membrane mineral scaling began to occur in the M3 tail membrane element just before triggering of feed flow reversal. In FFR mode, PV6 which was previously the tail element (when operating in NFF mode) became the lead RO element being exposed to the RO feed water. Toward the end of each FFR period permeate flux from the lead element increased slightly from ~27 to 28.5 L/h·m^2 to ~29–30 L/h·m^2. This permeate flux increase is indicative of gypsum crystal dissolution (from PV6 which was previously scaled in the NFF operational period) due to exposure of the PV6 membrane surface to the gypsum undersaturated feed water. As the feed flow reverted to the forward direction (NFF), permeate flux for PV6 (lead element in FFR) recovered toward its initial tail element value at the beginning of the new NFF period (29.1–30.2 L/h·m^2). Except for one cycle (#11), permeate flux recovery (based on PV6) was always restored to within 5% of the initial permeate flux which was set as that measured at the beginning of the test (Fig. 10). Overall, within the accuracy of permeate flux measurements, the cyclic M3 system operation was robust without persistent flux decline due to scaling.

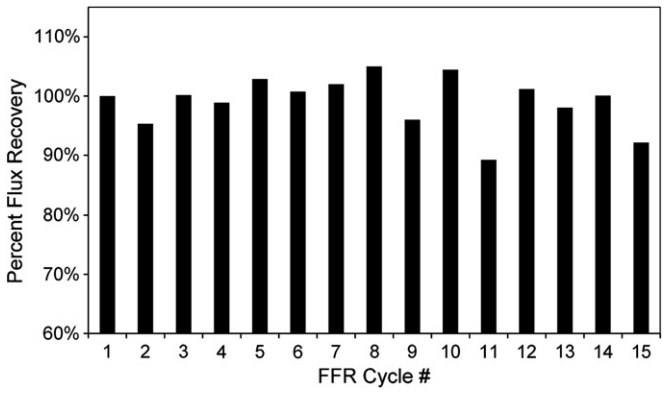

Fig. 10. Percent recovery for the tail element (PV6) permeate flux for the series of FFR cycles for Test #2 (69% recovery for period of 88 h, $SI_{gm} = 2.76$; Table 3).

3.3. FFR cycle period and frequency

The FFR cycle time, defined as the sum of the NFF and FFR operating times, varied in Test #2 (Table 3) from about 3 to 11 h (the average being 5.58 ± 3.76 h). Variability of the FFR cycle times should be expected since mineral salt nucleation on the membrane surface is a stochastic process [13,19]. Therefore, the rate of nucleation and seeding of crystals on the membrane surface can vary to some degree even for the same level of solution supersaturation. The above range of cycle period is reasonable as infrequent FFR triggering could lead to rapid progressive membrane scaling and thus loss of performance. Conversely, too frequent FFR triggering may result in pressure fluctuations that are difficult to control in addition to potential increase of valve maintenance cost due to heavy "duty cycle". From a practical viewpoint, variability of the triggering time for each FFR cycle highlights the importance of incorporating feedback control [21,23]. It also indicates that setting a fixed predetermined triggering time interval for a long-term desalting operation could result in FFR triggering that may occur prematurely or too late. Overall, Test #2 demonstrated that self-adaptive FFR can be effective in mitigating membrane mineral scaling under scaling operating conditions (Table 3, $SI_{gm} = 2.76$ for the M3) without antiscalant dosing (Fig. 11).

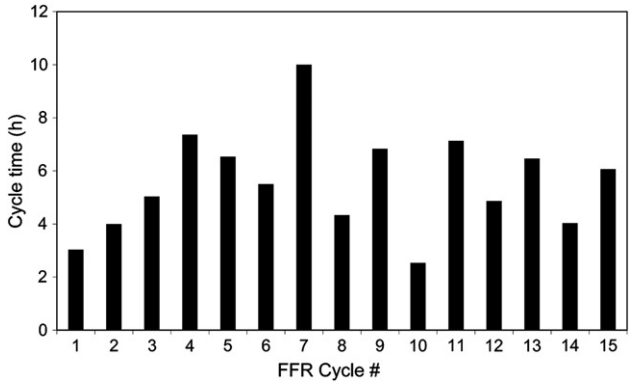

Fig. 11. FFR cell cycle periods over the course of Test #2 (M3 operation at 69% recovery for 88 h, $SI_{gm} = 2.76$; Table 3) demonstrating variability of FFR cycle times due to the stochastic nature of mineral scaling.

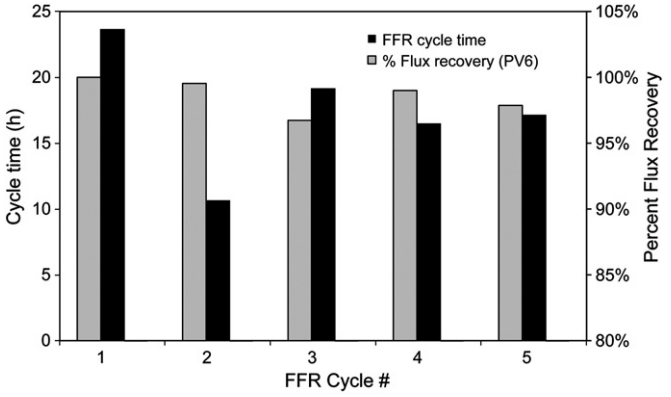

Fig. 13. FFR cell cycle periods for Test #3 (M3 operating at 81% recovery for 80 h, with the FFR trigger set to 65% surface scale coverage in the MeMo monitored area, Test #3, Table 3) demonstrating variability of FFR cycle times due to the stochastic nature of mineral scaling.

3.4. Self-adaptive FFR at high RO recovery

In order to further evaluate the feasibility of self-adaptive FFR operation at a higher recovery level, and thus greater mineral scaling propensity, the M3 pilot was operated at 81% recovery in Test #3. The gypsum saturation index at the membrane surface was 3.45, which is even above the level typically recommended for antiscalant dosing for gypsum scale suppression [24,25]. At this higher SI_{gm}, the FFR scaling threshold (set in the MeMo RO cell) was increased from 50% to 65% surface area scale coverage in the MeMo observation zone. The MeMo operating conditions were then set to attain $SI_{g,m} = 3.65$ (in the observation zone) which was higher by ~6% than in the spiral-wound tail element. The self-adaptive 80 h operation of Test #3 resulted in five cycles (Figs. 12 and 13) with a cycle time of 17.43 ± 8.25 h (Fig. 13), which (as expected) was significantly higher than in Test #2. The normalized flux for elements PV1 and PV6 (which alternated as being either the lead or tail element; Fig. 12) indicates repeated cycles where the initial flux of these elements PV6 was recovered (as observed by the initial flux of their respective NFF cycles). The initial tail element permeate flux for PV1 returned to 14.6–15.0 L/h·m^2 while the initial tail permeate flux for membrane element in PV 6 returned to flux values of 14.3–15.2 L/h·m^2. The initial permeate flux of PV1, when operating as the lead element after each FFR cycle, recovered to ~33 L/h·m^2 while the initial permeate flux for PV6 recovered to 32–33 L/h·m^2 when operating as the lead element. The normalized tail permeate flux recovery for PV6 was 98.3% ± 2.4% which was an excellent level of performance considering the fact that the FFR cycles were long. It is noted that FFR triggering was less aggressive than in Test #2 for which the FFR cycles were on the average about a factor of two shorter than in Test #3.

The present study demonstrated that self-adaptive operation of a spiral-wound RO plant, under conditions of high mineral scaling propensity, is technically feasible with the use of advanced mineral scale monitoring and integrated RO FFR plant control. Given that water feed quality may vary (over time), with respect to the concentration of sparingly water soluble mineral salts, self-adaptive FFR operation is essential for scale-free RO plant operation. Although the present study demonstrated that FFR can be effective without antiscalant use, there is merit in exploring FFR operation even with antiscalants use to reduce antiscalant dosage and thus allow higher

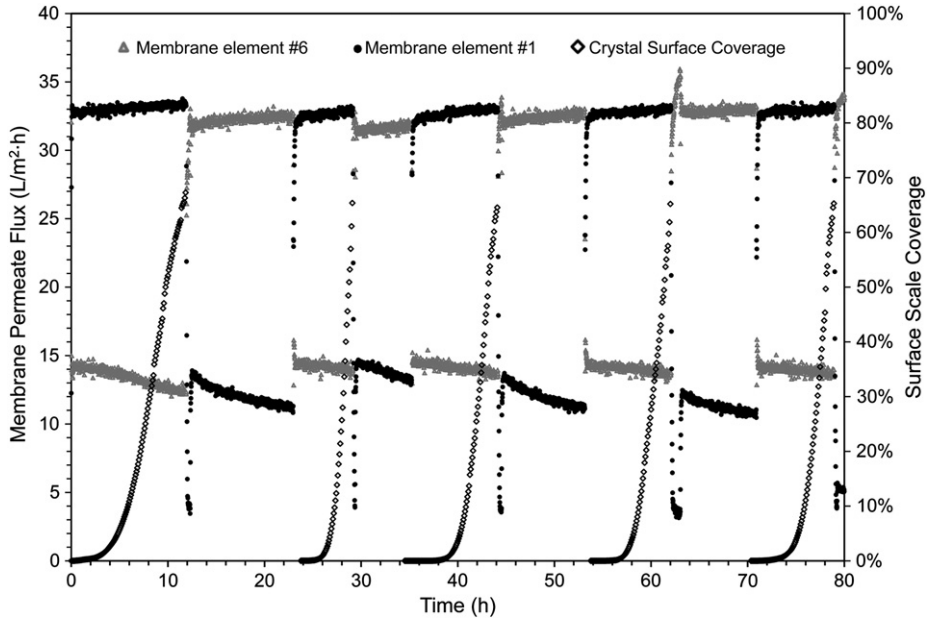

Fig. 12. Permeate flux (normalized) for membrane elements PV1 and PV6 during NFF and FFR periods, along with percent surface crystal coverage in the MeMo cell monitored area (M3 operation at 81% recovery with $SI_{gm} = 3.45$, with the FFR trigger set to 65% surface scale coverage in the MeMo monitored area, Test #3, Table 3).

level of recovery. Admittedly, long-term pilot testing will be required to assess the reliability of the approach under field conditions when scaling can be due to multiplicity of different mineral scalants.

4. Conclusions

The technical feasibility of operating a spiral-wound RO desalting process in a cyclic mode of feed-flow reversal (FFR) was evaluated using an automated RO pilot system interfaced with an online external membrane monitor (MeMo). Real time detection of mineral scaling enabled self-adaptive FFR operation which was accomplished by feed-back control with FFR triggering based on a threshold level of mineral scaling in the MeMo RO cell. Cyclic FFR RO operation at a high permeate product recovery, under conditions of gypsum supersaturation at the membrane surface, was feasible without antiscalant addition while achieving effective scale mitigation without interruption of permeate productivity. FFR operation of spiral-wound RO plant was effective even with the initiation of membrane cleaning (i.e., via FFR) after measurable level of scale formation in the MeMo and spiral-wound pilot. Variations in the length of FFR cycles were encountered and attributed to the stochastic nature of crystal nucleation on the membrane surface demonstrating the need for real-time feedback control. Although the adoption of FFR for scale-free RO plant operation is appealing, there are a number of key issues that need to be addressed via systematic studies including: (a) resilience and performance of the membranes in the RO plant and the MeMo cell when subjected to long-term multi-cycle FFR operation of scaling and scale dissolution; and (b) FFR effectiveness under field conditions involving multiplicity of different mineral scalants; and (c) feed-back control of FFR with added redundancy (in the event of failure of online MeMo membrane surface image analysis) to allow for triggering of FFR based on permeate flux decline monitoring from both the tail element and the MeMo cell.

Acknowledgments

This work was supported in part, by the California Department of Water Resources, the United States Environmental Protection Agency, the National Water Research Institute, the Office of Naval Research, and the UCLA Water Technology Research Center. The authors also acknowledge Dr. Jack Gilron for valuable discussions regarding the concept of RO operation in the mode of feed flow reversal.

References

[1] N.H. Lin, M.M. Kim, G.T. Lewis, Y. Cohen, Polymer surface nano-structuring of reverse osmosis membranes for fouling resistance and improved flux performance, J. Mater. Chem. 20 (2010) 4642–4652.
[2] A.H. Zhu, A. Rahardianto, P.D. Christofides, Y. Cohen, Reverse osmosis desalination with high permeability membranes — Cost optimization and research needs, Desalin. Water Treat. 15 (2009) 256–266.
[3] M. Wilf, Future of the osmotic processes, Desalin. Water Treat. 15 (2009) 292–298.
[4] A.H. Zhu, P.D. Christofides, Y. Cohen, On RO membrane and energy costs and associated incentives for future enhancements of membrane permeability, J. Membr. Sci. 344 (2009) 1–5.
(ibid, Corrigendum - 346 (2009) 2361)
[5] C. Fritzmann, J. Lowenberg, T. Wintgens, T. Melin, State-of-the-art of reverse osmosis desalination, Desalination 216 (2007) 1–76.
[6] A.R. Bartman, A.H. Zhu, P.D. Christofides, Y. Cohen, Minimizing energy consumption in reverse osmosis membrane desalination using optimization-based control, J. Process Control 20 (2010) 1261–1269.
[7] A. Joss, C. Baenninger, P. Foa, S. Koepke, M. Krauss, C.S. McArdell, K. Rottermann, Y.S. Wei, A. Zapata, H. Siegrist, Water reuse: >90% water yield in MBR/RO through concentrate recycling and CO2 addition as scaling control, Water Res. 45 (2011) 6141–6151.
[8] M. Uchymiak, A. Rahardianto, E. Lyster, J. Glater, Y. Cohen, A novel RO ex situ scale observation detector (EXSOD) for mineral scale characterization and early detection, J. Membr. Sci. 291 (2007) 86–95.
[9] R.W. Lee, J. Glater, Y. Cohen, C. Martin, K. Kovac, M.N. Milobar, D.W. Bartel, Low-pressure RO membrane desalination of agricultural drainage water, Desalination 155 (2003) 109–120.
[10] B.C. McCool, A. Rahardianto, J. Faria, K. Kovac, D. Lara, Y. Cohen, Feasibility of reverse osmosis desalination of brackish agricultural drainage water in the San Joaquin Valley, Desalination 261 (2010) 240–250.
[11] A. Rahardianto, W.Y. Shih, R.W. Lee, Y. Cohen, Diagnostic characterization of gypsum scale formation and control in RO membrane desalination of brackish water, J. Membr. Sci. 279 (2006) 655–668.
[12] E. Lyster, M.M. Kim, J. Au, Y. Cohen, A method for evaluating antiscalant retardation of crystal nucleation and growth on RO membranes, J. Membr. Sci. 364 (2010) 122–131.
[13] N. Pomerantz, Y. Ladizhansky, E. Korin, M. Waisman, N. Daltrophe, J. Gilron, Prevention of scaling of reverse osmosis membranes by "zeroing" the elapsed nucleation time. Part I. Calcium sulfate, Ind. Eng. Chem. Res. 45 (2006) 2008–2016.
[14] J. Gilron, M. Waisman, N. Daltrophe, N. Pomerantz, M. Milman, I. Ladizhansky, E. Korin, Prevention of precipitation fouling in NF/RO by reverse flow operation, Desalination 199 (2006) 29–30.
[15] E. Lyster, J. Au, R. Rallo, F. Giralt, Y. Cohen, Coupled 3-D hydrodynamics and mass transfer analysis of mineral scaling-induced flux decline in a laboratory plate-and-frame reverse osmosis membrane module, J. Membr. Sci. 339 (2009) 39–48.
[16] M. Uchymiak, A.R. Bartman, N. Daltrophe, M. Weissman, J. Gilron, P.D. Christofides, W.J. Kaiser, Y. Cohen, Brackish water reverse osmosis (BWRO) operation in feed flow reversal mode using an ex situ scale observation detector (EXSOD), J. Membr. Sci. 341 (2009) 60–66.
[17] N. Avraham, C. Dosoretz, R. Semiat, Osmotic backwash process in RO membranes, Desalination 199 (2006) 387–389.
[18] J.-J. Qin, M.H. Oo, K.A. Kekre, B. Liberman, Development of novel backwash cleaning technique for reverse osmosis in reclamation of secondary effluent, J. Membr. Sci. 346 (2009) 8–14.
[19] M. Uchymiak, E. Lyster, J. Glater, Y. Cohen, Kinetics of gypsum crystal growth on a reverse osmosis membrane, J. Membr. Sci. 314 (2008) 163–172.
[20] A.R. Bartman, E. Lyster, R. Rallo, P.D. Christofides, Y. Cohen, Mineral scale monitoring for reverse osmosis desalination via real-time membrane surface image analysis, Desalination 273 (2011) 64–71.
[21] A.R. Bartman, C.W. McFall, P.D. Christofides, Y. Cohen, Model-predictive control of feed flow reversal in a reverse osmosis desalination process, J. Process Control 19 (2009) 433–442.
[22] OLI Systems, OLI Analyzer 2.0, Morris Plains, NJ, , 2005..
[23] A.R. Bartman, P.D. Christofides, Y. Cohen, Nonlinear model-based control of an experimental reverse-osmosis water desalination system, Ind. Eng. Chem. Res. 48 (2009) 6126–6136.
[24] ROSA, Dow Water Solutions, 2010.
[25] Filmtec Reverse Osmosis Membranes Technical Manuals, Dow Water Solutions, 2009.